Focusing with plane time-reversal mirrors: An efficient alternative to closed cavities

Didier Cassereau and Mathias Fink
Laboratoire Ondes et Acoustique, Université Paris VII, E.S.P.C.I., 10 rue Vauquelin, 75231 Paris Cedex 05, France

(Received 17 September 1992; accepted for publication 21 June 1993)

In this paper, a theoretical foundation is proposed and numerical results are provided for focusing by plane, time-reversal mirrors of finite dimensions in a homogeneous fluid. The basic ideas are the same as those used in the *closed time-reversal cavity* (CTRC) system [Cassereau *et al.*, Proc. IEEE Ultrason. Symp., 1613–1618 (1990); D. Cassereau and M. Fink, IEEE Trans. Ultrason. Ferroelec. Freq. Control **39**, 579–592 (1992)], except that the most unrealistic assumptions made in this theoretical approach are dropped. Plane mirrors are considered that do not surround the object source, and different kinds of radiation conditions are introduced on the surface of these mirrors, in order to obtain more realistic situations from an experimental point of view. The results are compared with those of the CTRC system and it is shown how the focal pattern is changed in comparison with the pattern of the theoretical (and ideal) model. The differences between several radiation conditions on the surface of the mirror are also analyzed. The theory is based on a time domain formulation of diffraction, but a frequency analysis provides closed form solutions in some particular cases. Numerical results show that plane time-reversal mirrors of finite dimensions represent an efficient and realistic alternative to the CTRC system.

PACS numbers: 43.20.Fn, 43.20.Px, 43.20.Bi

INTRODUCTION

One of the most significant problems in propagation of acoustic waves lies in wave front or phase distortion correction. For example, it is always difficult to focus an acoustic field on a target after propagation in an inhomogeneous medium. Indeed, the inhomogeneities generate a distortion of the incident wave front, such that the knowledge of the spatial localization of a target is not enough to optimize focusing on it.

Among the different techniques proposed to solve this problem, the time-reversal method provides encouraging experimental as well as theoretical results.[1–5] The basic principle of the time-reversal method is based on a classical property of the wave equation in a lossless propagation medium: the time derivative operator appears to the second order only,[1–5] such that if $p(\mathbf{r},t)$ is a solution, then $p(\mathbf{r},-t)$ is also a solution of the same equation. In other words, the wave equation is unchanged by the time-reversal transform if there is no absorption. The basic idea consists of a two-step process:[1–5] First, the target is considered as an active source that generates an acoustic field $p(\mathbf{r},t)$ that is subsequently recorded, and second, the information contained in this field is then used to try to generate $p(\mathbf{r},-t)$. The theoretical limitations of the method have been predicted in a work published recently about focusing using the CTRC system.[2,5] In this work, the cavity is assumed to be a closed surface surrounding the medium of interest. Each point on the surface of the cavity is assumed able to measure the pressure field and its normal derivative generated by the active source inside the cavity. During the second step, the source *is removed or remains passive* and it is possible to create secondary sources on the surface of the cavity (monopole and dipole sources), such that the boundary conditions on the surface of the cavity exactly correspond to the time-reversal of the components measured during the first step. In this theoretical context, it is shown how the pressure field generated during the second step is focused on the initial source position after propagation in a homogeneous or inhomogeneous fluid.[2,5] This theoretical work is interesting, but it is not very realistic from an experimental point of view due to the following reasons.

(i) In the reception mode, the ultrasonic transducer cannot simultaneously measure the pressure field and its normal derivative.

(ii) In the transmission mode, it is not possible to simultaneously impose the pressure and its normal derivative.

(iii) The reception and re-transmission operations cannot be performed at each point of the surface of the cavity; ultrasonic transducers have finite apertures, resulting in spatial filtering of the incident acoustic field.

(iv) The closed surface surrounding the region of interest is not easy to realize experimentally.

These are the reasons why the CTRC system must be considered as a theoretical approach to the analysis of the intrinsic limitations due to propagation and diffraction of the process.[2,5]

In this paper, we start with the theoretical description of the CTRC system and progressively modify it in order to eliminate the most unrealistic assumptions. During this process, we show how the efficiency of the focusing by time-reversal is altered. First, we consider a plane time-reversal mirror instead of a closed cavity. During the first

 0001-4966/93/94(4)/2373/14/$6.00

step of the process, each point of the mirror is assumed to be able to measure the incident acoustic pressure, its normal derivative or both. During the second step, we create secondary sources (monopole sources, dipole sources or both) according to the same basic idea as in the case of the CTRC system. Then, the time-reversed pressure field is computed near the initial source position using the impulse diffraction theory. The dimensions of the mirror are assumed to be finite.

In the first section, we develop the basic transient theory of the time-reversal process. Then, we distinguish between the following radiation conditions on the surface of the mirror.

(I) The time-reversal mirror is mounted on an infinite rigid planar baffle: in the first step, each point on the surface of the mirror measures the normal derivative of the incident acoustic pressure field; in the second step, this field is time-reversed and then re-transmitted.

(II) The time-reversal mirror is mounted on an infinite soft planar baffle: in the first step, each point on the surface of the mirror measures the incident acoustic pressure field; in the second step, this field is time-reversed and then re-transmitted.

(III) The time-reversal mirror behaves as it would in free-space: in the first step, each point on the surface of the mirror measures simultaneously the incident acoustic pressure field and its normal derivative; in the second step, these two components are time-reversed and then re-transmitted.

(IV) The time-reversal mirror is mounted on an infinite rigid planar baffle: in the first step, each point on the surface of the mirror measures the incident acoustic pressure field; in the second step, the normal derivative of the re-transmitted pressure field results from the time-reversal of the components measured in the first step.

For these different radiation conditions on the surface of the mirror, we derive and compare the expressions obtained for the time-reversed pressure field. Case IV is interesting since it corresponds, according to the previous remarks made about the limitations of the CTRC system, to the most realistic configuration when compared with experimental conditions.[2,5] In the second section, a frequency analysis of the results obtained in the first part is provided. This analysis allows an additional interpretation of the differences between the expressions of the time-reversed pressure field depending on the radiation conditions on the surface of the mirror.

The third section considers some particular cases where a closed form solution for the time-reversed pressure field is available. These closed form solutions allow a description of the time-reversed pressure field in terms of two wave fronts. These wave fronts are separated in time far from the initial source position, while they can overlap in the neighborhood of the origin. These results are compared to those obtained with the CTRC system. Finally, it is shown how the application of one mirror on each side of the source increases the performance of the focusing by time-reversal.

In the fourth and last section, we present numerical results and analyze the influence of different parameters (size of the time-reversal mirror and radiation conditions on its surface) on the focal pattern.

I. BASIC TRANSIENT THEORY

Similar to the theory of the CTRC system, we consider, during the first step (recording mode), a point-like source located at the origin of a spatial coordinate system, as illustrated in Fig. 1 (throughout this paper, we will use the word source both when considering step I and step II, ever though the source is acoustically inactive during step II). As this source is considered to be located inside an unbounded homogeneous fluid, it generates a scalar pressure field, $p(\mathbf{r},t)$, that satisfies the wave equation formulated in the time domain as[6]

$$\left(\nabla^2-\frac{1}{c^2}\partial_{tt}\right)p(\mathbf{r},t)=-\phi(t)\delta(\mathbf{r}), \tag{1}$$

where ∂_{tt} is the differential operator defined by $\partial_{tt}=\partial^2/\partial t^2$ and c is the sound speed. Here, ∇^2 represents the Laplacian operator with respect to the $\mathbf{r}$ coordinates [the scalar (x,y,z) and cylindrical (r,θ,z) coordinates will be used], $\delta(\mathbf{r})$ is the Dirac distribution in three-dimensional (3-D) space, and $\phi(t)$ is any function of time that describes the temporal variations of the source excitation. This function of time is assumed to be causal [i.e., $\phi(t)=0$ for $t<0$] and defined within a finite time interval $[0,T_\phi]$ [i.e., $\phi(t)=0$ for $t>T_\phi$].[2,5] Since the pressure field $p(\mathbf{r},t)$ propagates in a free unbounded homogeneous fluid, the solution to (1) can be found as[6]

$$p(\mathbf{r},t)=\frac{1}{4\pi|\mathbf{r}|}\phi\left(t-\frac{|\mathbf{r}|}{c}\right)=g_f(\mathbf{r},t)\overset{*}{t}\phi(t). \tag{2}$$

In this equation, $*/t$ represents the time-convolution operator and $g_f(\mathbf{r},t)$, defined by

$$g_f(\mathbf{r},t)=\frac{1}{4\pi|\mathbf{r}|}\delta\left(t-\frac{|\mathbf{r}|}{c}\right),$$

is the free-space Green's function; the latter corresponds to a diverging spherical impulse wave and satisfies (1) as well, when $\phi(t)$ is replaced by $\delta(t)$ on the right-hand side of the expression.[6]

The recording surface $\mathcal{S}$ is included in the plane Π defined by $z=z_0$ with $z_0>0$, as illustrated in Fig. 1. This plane is divided into two complementary parts and is written $\Pi=\mathcal{S}+\mathcal{P}$, where $\mathcal{S}$ corresponds to the active aperture surface of the time-reversal mirror. We introduce the aperture function of the mirror, $o(x,y)$, as follows:

$$o(x,y)=\begin{cases}1, & \text{if } \mathbf{r}(x,y,z_0)\in\mathcal{S},\\ 0, & \text{otherwise, i.e., if } \mathbf{r}(x,y,z_0)\in\mathcal{P}.\end{cases}$$

As in the case for the CTRC system, we also assume that the plane time-reversal mirror does not perturb the propagation of the pressure field, such that the infinite free-space hypothesis remains valid.[2,5]

In the following, we consider the surface of the time-reversal mirror to be finite. This assumption is important since it permits introduction of a time parameter T such

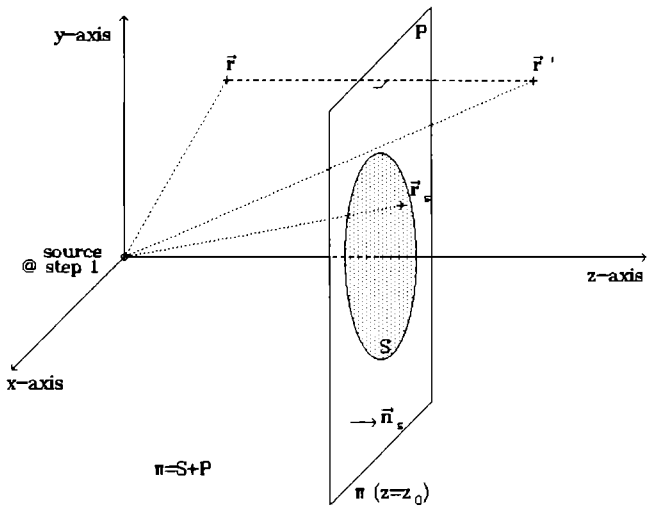

FIG. 1. Spatial coordinate system, $\mathbf{r}$ is the observation point of the acoustic field, $\mathbf{r}'$ is the mirror of $\mathbf{r}$ with respect to the plane Π, $\mathbf{r}_s$ is a point on the surface $\mathscr{S}$ of the time-reversal mirror and $\mathbf{n}_s$ is the normal vector to Π.

that the pressure field $p(\mathbf{r},t)$ vanishes everywhere on $\mathscr{S}$ for any observation time $t>T$: $p(\mathbf{r},t)=0(\forall \mathbf{r}\in\mathscr{S},\ \forall t>T)$.

Defining d_m as the greatest distance from the source to any point on the surface of the time-reversal mirror $\mathscr{S}$, $d_m=\max_{\mathbf{r}\in\mathscr{S}}(|\mathbf{r}|)$, T equals at least $(T_\phi+d_m/c)$, where d_m/c is the maximum time of propagation from the source to any point on the surface of the mirror. Once the parameter T is found according to this condition, the time-reversal mirror is assumed to be able to measure the pressure field and its normal derivative at any point of its surface during the time interval $[0,T]$. As for the CTRC system, we can imagine an infinite set of elementary transducers on the surface $\mathscr{S}$ of the mirror that measure the pressure field and its normal derivative without perturbing the field.[2,5]

During the second step of the process (transmission mode), we assume that we are able to create secondary sources on the surface of the mirror (monopole and dipole sources) such that the boundary conditions on the surface $\mathscr{S}$ correspond to the time-reversed components of the pressure field recorded during the first step. To insure causality, the time-reversal process is described by the transformation $t\Rightarrow T-t$ and the secondary sources are described as follows:[2,5]

$$\sigma_1(\mathbf{r}_s,t)=p(\mathbf{r}_s,T-t),\quad \sigma_0(\mathbf{r}_s,t)=\mathbf{n}_s\cdot\nabla_s p(\mathbf{r}_s,T-t). \tag{3}$$

The two functions σ_1 and σ_0 correspond to the pressure field and its normal derivative on the surface of the mirror, respectively, and are measured in Pa and $\mathrm{Pa}\cdot\mathrm{m}^{-1}$. In (3), $\mathbf{r}_s$ represents any point on the surface of the mirror, $\mathbf{n}_s$ is the normal vector to the plane Π as illustrated in Fig. 1, and $\mathbf{n}_s\cdot\nabla_s$ is the normal derivative operator. It is important to note that σ_1 and σ_0 are only valid on the surface of the mirror $\mathscr{S}$; they can be completely different on the surface $\mathscr{P}$ and we are not interested in their expressions.

Since the time-reversal mirror is included in the plane Π defined by $z=z_0$, the normal derivative operator $\mathbf{n}_s\cdot\nabla_s$ reduces, within a sign $\epsilon=\pm1$ (orientation convention), to the partial derivative operator with respect to the z_s coordinate. In the following, the time-reversed pressure field resulting from the new boundary conditions on the surface $\mathscr{S}$ is computed in front of the mirror, corresponding to the half-space $z<z_0$. According to the convention generally used in diffraction theory,[6–11] the normal vector $\mathbf{n}_s$ is oriented outward (in direction of increasing values of z), such that $\epsilon=+1$. It follows therefore that the secondary sources created on the surface of the mirror $\mathscr{S}$ are:

$$\begin{aligned}\sigma_1(\mathbf{r}_s,t)&=\frac{1}{4\pi|\mathbf{r}_s|}\,\phi\!\left(T-t-\frac{|\mathbf{r}_s|}{c}\right),\\ \sigma_0(\mathbf{r}_s,t)&=-\frac{z_0}{4\pi|\mathbf{r}_s|^2}\left[\frac{1}{|\mathbf{r}_s|}\,\phi\!\left(T-t-\frac{|\mathbf{r}_s|}{c}\right)\right.\\ &\quad\left.+\frac{1}{c}\,\phi'\!\left(T-t-\frac{|\mathbf{r}_s|}{c}\right)\right],\end{aligned} \tag{4}$$

where $\phi'(t)$ is defined as the temporal derivative of the excitation function $\phi(t)$.

The point-like source considered during the first step is *now removed or remains passive.* It follows from the new boundary conditions on the surface of the mirror $\mathscr{S}$ that a time-reversed pressure field, $p_{\mathrm{tr}}(\mathbf{r},t)$, is radiated from the mirror. Starting with Green's formulation of diffraction,[6,9–11] $p_{\mathrm{tr}}(\mathbf{r},t)$ can be found as

$$\begin{aligned}p_{\mathrm{tr}}(\mathbf{r},t)=\int_\Pi\left[\sigma_0(\mathbf{r}_s,t)\overset{*}{\underset{t}{}}g(\mathbf{r},\mathbf{r}_s,t)\right.\\ \left.-\sigma_1(\mathbf{r}_s,t)\overset{*}{\underset{t}{}}\mathbf{n}_s\cdot\nabla_s g(\mathbf{r},\mathbf{r}_s,t)\right]dx_s\,dy_s,\end{aligned} \tag{5}$$

where $g(\mathbf{r},\mathbf{r}_s,t)$ is the Green's function adapted to the radiation conditions on the surface of the mirror. We will now show how the diffraction pattern is modified by considering four different baffle conditions.

Case I: The time-reversal mirror is mounted on an infinite rigid planar baffle. In this situation, it can be shown that the Green's function corresponding to this baffle condition contains two free-space Green's functions at two different spatial locations and can be written as[9–11]

$$g(\mathbf{r},\mathbf{r}_s,t)=g_f(\mathbf{r}-\mathbf{r}_s,t)+g_f(\mathbf{r}'-\mathbf{r}_s,t), \tag{6a}$$

where the point $\mathbf{r}'$ is the mirror of the point $\mathbf{r}$ with respect to the plane Π; it is defined by the coordinates $\mathbf{r}'(x,y,2z_0-z)$. Using (6a), we obtain the following equations, valid for any point $\mathbf{r}_s$ on Π:

$$g(\mathbf{r},\mathbf{r}_s,t)=2g_f(\mathbf{r}-\mathbf{r}_s,t),\quad \mathbf{n}_s\cdot\nabla_s g(\mathbf{r},\mathbf{r}_s,t)=0. \tag{6b}$$

It also follows from the baffle condition that the normal derivative of the acoustic pressure $\sigma_0(\mathbf{r}_s,t)$ vanishes everywhere on the plane Π outside the surface of the time-reversal mirror $\mathscr{S}$ and we obtain the following equation, valid for any point $\mathbf{r}_s$ on $\mathscr{P}$:[9–11]

$$\sigma_0(\mathbf{r}_s,t)=0,\quad \forall \mathbf{r}_s\in\mathscr{P}. \tag{6c}$$

Introducing (6b) and (6c) in the expression for the time-reversed pressure field given by (5), we obtain

$$p_{tr}^{(1)}(\mathbf{r},t)=2\int_{\mathscr{S}}\sigma_0(\mathbf{r}_s,t)\overset{*}{\underset{t}{}}g_f(\mathbf{r}-\mathbf{r}_s,t)\,dx_s\,dy_s$$
$$=\frac{1}{2\pi}\int_{\mathscr{S}}\frac{1}{|\mathbf{r}-\mathbf{r}_s|}\sigma_0\left(\mathbf{r}_s,t-\frac{|\mathbf{r}-\mathbf{r}_s|}{c}\right)dx_s\,dy_s. \tag{6d}$$

Looking at (6d), we note that the time-reversed pressure field, $p_{tr}^{(1)}(\mathbf{r},t)$, only depends on σ_0 on the surface of the mirror $\mathscr{S}$. In particular, $p_{tr}^{(1)}(\mathbf{r},t)$ does not depend on σ_1 on the plane Π. Introducing (4) into (6d), we obtain

$$p_{tr}^{(1)}(\mathbf{r},t)=-\frac{z_0}{8\pi^2}\int_{\mathscr{S}}\frac{dx_s\,dy_s}{|\mathbf{r}_s|^2\times|\mathbf{r}-\mathbf{r}_s|}$$
$$\times\left[\frac{1}{|\mathbf{r}_s|}\phi\left(T-t+\frac{|\mathbf{r}-\mathbf{r}_s|-|\mathbf{r}_s|}{c}\right)\right.$$
$$\left.+\frac{1}{c}\phi'\left(T-t+\frac{|\mathbf{r}-\mathbf{r}_s|-|\mathbf{r}_s|}{c}\right)\right]. \tag{6e}$$

Case II: The time-reversal mirror is mounted on an infinite soft planar baffle; this case is analogous to the diffraction by an opaque screen in optics.[7,8] This situation is very similar to the previous case and the Green's function corresponding to this baffle condition contains the same two terms as (6a) and can be written as (note the "−" sign)

$$g(\mathbf{r},\mathbf{r}_s,t)=g_f(\mathbf{r}-\mathbf{r}_s,t)-g_f(\mathbf{r}'-\mathbf{r}_s,t). \tag{7a}$$

Treating (7a) in the same way as (6a) provides us with the following equations, valid for any point $\mathbf{r}_s$ on Π:

$$g(\mathbf{r},\mathbf{r}_s,t)=0,\quad \mathbf{n}_s\cdot\nabla_s g(\mathbf{r},\mathbf{r}_s,t)=2\mathbf{n}_s\cdot\nabla_s g_f(\mathbf{r}-\mathbf{r}_s,t). \tag{7b}$$

It also follows from the baffle condition that the acoustic pressure $\sigma_1(\mathbf{r}_s,t)$ vanishes everywhere on the plane Π outside the surface of the time-reversal mirror $\mathscr{S}$ and we obtain the following equation, valid for any point $\mathbf{r}_s$ on $\mathscr{P}$:[7,8]

$$\sigma_1(\mathbf{r}_s,t)=0,\quad \forall\mathbf{r}_s\in\mathscr{P}. \tag{7c}$$

Introducing (7b) and (7c) in the expression for the time-reversed pressure field given by (5), we obtain

$$p_{tr}^{(2)}(\mathbf{r},t)=-2\int_{\mathscr{S}}\sigma_1(\mathbf{r}_s,t)\overset{*}{\underset{t}{}}\mathbf{n}_s\cdot\nabla_s g_f(\mathbf{r}-\mathbf{r}_s,t)\,dx_s\,dy_s, \tag{7d}$$

where the normal derivative of the free-space Green's function is given by

$$\mathbf{n}_s\cdot\nabla_s g_f(\mathbf{r}-\mathbf{r}_s,t)$$
$$=\frac{\partial}{\partial z_s}\left[\frac{1}{4\pi|\mathbf{r}-\mathbf{r}_s|}\delta\left(t-\frac{|\mathbf{r}-\mathbf{r}_s|}{c}\right)\right]$$
$$=-\frac{z_0-z}{4\pi|\mathbf{r}-\mathbf{r}_s|^2}\left[\frac{1}{|\mathbf{r}-\mathbf{r}_s|}\delta\left(t-\frac{|\mathbf{r}-\mathbf{r}_s|}{c}\right)\right.$$
$$\left.+\frac{1}{c}\delta'\left(t-\frac{|\mathbf{r}-\mathbf{r}_s|}{c}\right)\right]. \tag{7e}$$

Looking at (7d) and (7e), we note that the time-reversed pressure field, $p_{tr}^{(2)}(\mathbf{r},t)$, now depends on σ_1 on the surface of the mirror $\mathscr{S}$. We also specifically note that $p_{tr}^{(2)}(\mathbf{r},t)$ does not depend on σ_0 on the plane Π. Finally, introducing (4) and (7e) into (7d) yields

$$p_{tr}^{(2)}(\mathbf{r},t)=\frac{z_0-z}{8\pi^2}\int_{\mathscr{S}}\frac{dx_s\,dy_s}{|\mathbf{r}_s|\times|\mathbf{r}-\mathbf{r}_s|^2}$$
$$\times\left[\frac{1}{|\mathbf{r}-\mathbf{r}_s|}\phi\left(T-t+\frac{|\mathbf{r}-\mathbf{r}_s|-|\mathbf{r}_s|}{c}\right)\right.$$
$$\left.-\frac{1}{c}\phi'\left(T-t+\frac{|\mathbf{r}-\mathbf{r}_s|-|\mathbf{r}_s|}{c}\right)\right]. \tag{7f}$$

Case III: The pressure field propagates on both sides of plane Π and the time-reversal mirror does not perturb the propagation. In this case, the Green's function corresponding to this radiation condition reduces to the free-space Green's function. Looking at cases I and II described above, it appears clearly that the diffracted pressure field only depends on the acoustic pressure and its normal derivative on the surface of the time-reversal mirror, such that it was not necessary to determine the expressions of $\sigma_0(\mathbf{r}_s,t)$ and/or $\sigma_1(\mathbf{r}_s,t)$ outside $\mathscr{S}$ [remember that the expressions given in (3) are only valid on the surface of the mirror $\mathscr{S}$]. However, in the case of the free-space Green's function, such a simplification is not possible. By carrying out the integration over the planes $\mathscr{S}$ and $\mathscr{P}$ separately, we obtain from (5):

$$p_{tr}^{(3)}(\mathbf{r},t)=\int_{\mathscr{S}}\sigma_0(\mathbf{r}_s,t)\overset{*}{\underset{t}{}}g_f(\mathbf{r}-\mathbf{r}_s,t)\,dx_s\,dy_s$$
$$-\int_{\mathscr{S}}\sigma_1(\mathbf{r}_s,t)\overset{*}{\underset{t}{}}\mathbf{n}_s\cdot\nabla_s g_f(\mathbf{r}-\mathbf{r}_s,t)\,dx_s\,dy_s$$
$$+\int_{\mathscr{P}}\left(\sigma_0(\mathbf{r}_s,t)\overset{*}{\underset{t}{}}g_f(\mathbf{r}-\mathbf{r}_s,t)\right.$$
$$\left.-\sigma_1(\mathbf{r}_s,t)\overset{*}{\underset{t}{}}\mathbf{n}_s\cdot\nabla_s g_f(\mathbf{r}-\mathbf{r}_s,t)\right)dx_s\,dy_s. \tag{8a}$$

Comparing (8a) with the equations written in cases I and II, the time-reversed pressure field can be simplified as follows:

$$p_{tr}^{(3)}(\mathbf{r},t)=\frac{1}{2}p_{tr}^{(1)}(\mathbf{r},t)+\frac{1}{2}p_{tr}^{(2)}(\mathbf{r},t)$$
$$+\int_{\mathscr{P}}\left(\sigma_0(\mathbf{r}_s,t)\overset{*}{\underset{t}{}}g_f(\mathbf{r}-\mathbf{r}_s,t)\right.$$
$$\left.-\sigma_1(\mathbf{r}_s,t)\overset{*}{\underset{t}{}}\mathbf{n}_s\cdot\nabla_s g_f(\mathbf{r}-\mathbf{r}_s,t)\right)dx_s\,dy_s. \tag{8b}$$

As a consequence, the time-reversed pressure field reduces to half the sum of the pressure fields diffracted for cases I and II (rigid and soft baffle conditions), up to a correction term corresponding to the integral over the surface $\mathscr{P}$.

This correction term is clearly due to the finite size of the time-reversal mirror $\mathscr{S}$.

Case IV: The time-reversal mirror is mounted on an infinite rigid planar baffle, but the normal derivative of the acoustic pressure on the surface of the mirror during the second step is assumed proportional to the time-reversal of the incident pressure. This case is interesting since the most commonly used approximations for characterization of ultrasonic transducers are the following.[9–12]

(i) A transducer working in receiving mode essentially measures the average incident acoustic pressure on its surface.

(ii) A transducer working in transmission mode essentially imposes the velocity distribution components that are perpendicular to the aperture surface on its surroundings (if ρ is the density of the propagation fluid, the normal velocity vector and the normal derivative of the acoustic pressure on the surface of the transducer are identical, up to a constant $-\rho$ and a temporal derivative).

Although the time-reversal mirror, as described in this paper, cannot be realized experimentally, case IV is more realistic in comparison with time-reversal experiments that are performed in the laboratory using transducer arrays.[1–5]

Since the baffle is assumed to be rigid, the results are very similar to those obtained in case I; it is enough to replace the expression of $\sigma_0(\mathbf{r}_s,t)$ by $\sigma_1(\mathbf{r}_s,t)$ in (4). After some elementary computation steps that we do not present here in detail, we obtain the following expression of the time-reversed pressure field:

$$p_{\mathrm{tr}}^{(4)}(\mathbf{r},t)=\frac{1}{8\pi^2}\int_{\mathscr{S}}\frac{dx_s\,dy_s}{|\mathbf{r}_s|\times|\mathbf{r}-\mathbf{r}_s|}\times\phi\left(T-t+\frac{|\mathbf{r}-\mathbf{r}_s|-|\mathbf{r}_s|}{c}\right). \tag{9}$$

II. FREQUENCY ANALYSIS

In the previous section, the problem has been analyzed exclusively in the time domain. We will now perform a frequency analysis to complete the physical interpretation of the time-reversal process. We will use the following conventions:

(i) f is the frequency, linked to the time variable t via the Fourier transform;

(ii) f_x and f_y are the spatial frequencies, linked to x and y via the *spatial* two-dimensional Fourier transform;

(iii) a function of space is generally written as a function of $\mathbf{r}$; however sometimes it will be written as a function of the explicit coordinates (x,y,z);

(iv) if $u(x,y,z,t)$ is any function of time and space, $\tilde{u}(x,y,z,f)$ corresponds to its Fourier transform over t, $U(f_x,f_y,z,t)$ to its spatial two-dimensional Fourier transform over x and y, and $\tilde{U}(f_x,f_y,z,f)$ to its three-dimensional Fourier transform over x, y, and t.

We first compute the Fourier transform $\tilde{G}_f(f_x,f_y,z,f)$ of the free-space Green's function $g_f(x,y,z,t)$. The Fourier transform over the time variable t is

$$\tilde{g}_f(x,y,z,f)=\int_{-\infty}^{+\infty}\frac{1}{4\pi R}\delta\left(t-\frac{R}{c}\right)\exp(j2\pi ft)dt=\frac{1}{4\pi R}\exp\left(\frac{j2\pi fR}{c}\right),$$

where R is defined by $R=\sqrt{x^2+y^2+z^2}$. Since $\tilde{g}_f(x,y,z,f)$ is radial symmetric and only depends on $r=\sqrt{x^2+y^2}$, $\tilde{G}_f(f_x,f_y,z,f)$ is symmetric as well and only depends on $f_r=\sqrt{f_x^2+f_y^2}$. In this case, the spatial two-dimensional Fourier transform over x and y can be changed to a Hankel transform using the Bessel function of zeroth order:[13,14]

$$\tilde{G}_f(f_x,f_y,z,f)=2\pi\int_0^{+\infty}\frac{\exp(j2\pi fR/c)}{4\pi R}rJ_0(2\pi f_r r)dr.$$

This integral can be found in tables of integral transforms[15] and we obtain[16]

$$\tilde{G}_f(f_x,f_y,z,f)=(j/2\nu)\exp(j\nu|z|) \tag{10}$$

where ν, in units m^{-1}, is defined by

$$\nu=2\pi\times\begin{cases}\sqrt{f^2/c^2-f_r^2}, & \text{if } f_r<f/c,\\ j\sqrt{f_r^2-f^2/c^2}, & \text{if } f_r>f/c.\end{cases} \tag{11}$$

Note that (10) and (11) are only valid for positive values of the frequency f. For negative values of f, these equations must be re-written such that $\tilde{G}_f(f_x,f_y,z,f)$ is a Hermitic function of f [the free-space Green's function $g_f(x,y,z,t)$ takes only real values].[13,16] Looking at the expression in (11), we note that ν can be either real or purely imaginary. The real values of ν correspond to the propagating components in the angular spectrum of the free-space Green's function, while the purely imaginary values correspond to nonpropagating (evanescent) components with an amplitude that decreases exponentially with $|z|$.[16] Finally, it follows from (2) that the Fourier transform over x, y, and t of the pressure field $p(\mathbf{r},t)$ generated during the first step is given by[13]

$$\tilde{P}(f_x,f_y,z,f)=\tilde{G}_f(f_x,f_y,z,f)\tilde{\phi}(f). \tag{12}$$

Starting from (4), it follows from the basic properties of the convolution operator that the secondary source term (acoustic pressure) $\sigma_1(\mathbf{r}_s,t)$ can be written as follows:[13]

$$\sigma_1(\mathbf{r}_s,t)=\frac{1}{4\pi|\mathbf{r}_s|}\phi\left(T-t-\frac{|\mathbf{r}_s|}{c}\right)=\frac{1}{4\pi|\mathbf{r}_s|}\delta\left(t+\frac{|\mathbf{r}_s|}{c}\right)\overset{*}{t}\delta(t-T)\overset{*}{t}\phi(-t)=g_f(\mathbf{r}_s,-t)\overset{*}{t}\delta(t-T)\overset{*}{t}\phi(-t). \tag{13a}$$

Taking the Fourier transform of (13a) over the time variable t, we obtain

$$\tilde{\sigma}_1(\mathbf{r}_s,f)=\exp(j2\pi fT)\tilde{\phi}(f)^*\tilde{g}_f(\mathbf{r}_s,f)^*, \tag{13b}$$

where * indicates the complex conjugate. Therefore, it follows from (13b) and (10) that the spatial two-dimensional

Fourier transform, $\tilde{\Sigma}_1(f_x,f_y,z_0,f)$, of $\tilde{\sigma}_1(\mathbf{r}_s,f)$ over x_s and y_s is given by

$$\tilde{\Sigma}_1(f_x,f_y,z_0,f)=-\frac{j}{2}\left(\frac{1}{\nu}\exp(j\nu z_0)\right)^* \times\exp(j2\pi fT)\tilde{\phi}(f)^*. \tag{13c}$$

Since the secondary source term (the derivative of the acoustic pressure normal to the plane Π), $\sigma_0(\mathbf{r}_s,t)$, is linked to $\sigma_1(\mathbf{r}_s,t)$ by the relationship

$$\sigma_0(\mathbf{r}_s,t)=\frac{\partial}{\partial z_s}\sigma_1(\mathbf{r}_s,t)\,|_{z_s=z_0}, \tag{13d}$$

and z_s is not included in the Fourier transform of interest, (13d) can be used to modify (13c) to yield

$$\tilde{\Sigma}_0(f_x,f_y,z_0,f)=-\tfrac{1}{2}[\exp(j\nu z_0)]^*\exp(j2\pi fT)\tilde{\phi}(f)^*. \tag{13e}$$

We will now consider the four different cases from the previous section.

Case I: As stated previously in (6d), the time-reversed pressure field can be calculated by an integration over the surface $\mathcal{S}$ of the mirror; introducing the aperture function of the mirror $o(x,y)$ as defined in the first section, this integration can be extended to the complete plane Π at $z=z_0$, so that

$$p_{\mathrm{tr}}^{(1)}(\mathbf{r},t)=2\int_{\Pi}o(x_s,y_s)\sigma_0(x_s,y_s,z_0,t) \overset{*}{\frac{}{t}}g_f(x-x_s,y-y_s,z-z_0,t)\,dx_s\,dy_s. \tag{14a}$$

Next, this equation can be interpreted as a spatial convolution of $o(x,y)\sigma_0(x,y,z_0,t)$ with $g_f(x,y,z-z_0,t)$ over x and y, yielding the simplification:[13]

$$p_{\mathrm{tr}}^{(1)}(\mathbf{r},t)=2[o(x,y)\sigma_0(x,y,z_0,t)]\overset{*}{\frac{}{x}}\overset{*}{\frac{}{y}}\overset{*}{\frac{}{t}}g_f(x,y,z-z_0,t). \tag{14b}$$

Finally taking the Fourier transform of (14b) over x, y, and t, it follows from (10) and (13e), and from the basic properties of the Fourier transform with respect to the convolution operator, that[13]

$$\tilde{P}_{\mathrm{tr}}^{(1)}(f_x,f_y,z,f)=-\frac{j}{2\nu}\exp(j2\pi fT)\tilde{\phi}(f)^*\exp(j\nu z_0)\exp(-j\nu z) \times\left(O(f_x,f_y)\overset{*}{\frac{}{f_x}}\overset{*}{\frac{}{f_y}}\exp(j\nu z_0)^*\right). \tag{14c}$$

The main difficulty that arises in (14c) is the computation of the convolution over f_x and f_y. In general, we cannot obtain a closed form expression of the time-reversed pressure field $\tilde{P}_{\mathrm{tr}}^{(1)}(f_x,f_y,z,f)$ and the convolution must be performed numerically. It is noted though, that if the active aperture of the time-reversal mirror is infinite, i.e., $\mathcal{S}=\Pi$, we immediately obtain $o(x,y)=1(\forall x,y)$, such that $O(f_x,f_y)$ reduces to $\delta(f_x)\delta(f_y)$. In this case, the convolution is straightforward, but the finite-valued time parameter T introduced in the first section cannot be defined for a time-reversal mirror of infinite size. Furthermore, such a time-reversal mirror is not realistic experimentally.

Alternatively, the simplification of (14c) can be approached as follows. It is well known from the classical properties of the Fourier transform that a wide function has a narrow Fourier transform.[13] With this in mind, we will choose the size of the mirror (in both directions x and y), such that the spatial two-dimensional Fourier transform over x and y of the aperture function of the mirror, $O(f_x,f_y)$, is much more narrow than $\exp(j\nu z_0)^*$, where ν is given by (11). This choice of the mirror dimensions depends on the variations of $\exp(j\nu z_0)^*$ with f_x and f_y; consequently, it depends on the frequency f. Assuming that $O(f_x,f_y)\simeq\delta(f_x)\delta(f_y)$, (14c) can be simplified and written as follows:

$$\tilde{P}_{\mathrm{tr}}^{(1)}(f_x,f_y,z,f)\simeq-(j/2\nu)\exp(j2\pi fT)\tilde{\phi}(f)^* \times|\exp(j\nu z_0)|^2\exp(-j\nu z). \tag{14d}$$

We now replace ν by the expression given in (11) and obtain

$$\tilde{P}_{\mathrm{tr}}^{(1)}(f_x,f_y,z,f)\simeq-\frac{1}{4\pi}\exp(j2\pi fT)\tilde{\phi}(f)^*\begin{cases}\dfrac{j}{\sqrt{f^2/c^2-f_r^2}}\exp[-j2\pi z\sqrt{f^2/c^2-f_r^2}], & \text{if } f_r<f/c,\\ \dfrac{1}{\sqrt{f_r^2-f^2/c^2}}\exp[2\pi(z-2z_0)\sqrt{f_r^2-f^2/c^2}], & \text{if } f_r>f/c.\end{cases} \tag{14e}$$

From the spatial and temporal Fourier transform of the time-reversed pressure field in (14e), we can make the following observations.

(1) Comparing (14e) with (10), where (11) is inserted, we see that the propagating components ($f_r<f/c$) of the time-reversed pressure field have a form which is similar to the form of the complex conjugate of the pressure field generated by the source during the first step (the time-reversal process in the time domain is equivalent to a complex conjugation in the frequency domain).[17]

(2) In the neighborhood of $z=0$, the time-reversed pressure field only propagates in direction of decreasing

values of z [the term $\exp(-jvz)$ in (14d)], while the pressure field generated by the source during the first step propagates in both directions [the term $\exp(jv|z|)$ in (10), due to the spherical geometry of the wave front].

(3) The propagating components of the time-reversed pressure field do not depend on the position z_0 of the time-reversal mirror.

(4) The evanescent components of the time-reversed pressure field explicitly depend on z_0.

As a consequence, the pressure field radiated from the time-reversal mirror looks very similar to the complex conjugate of the pressure field generated by the initial source during the first step, resulting in a reconstruction of the initial wave front by time-reversal. But the above mentioned remarks also exhibit some differences that introduce limitations in the reconstruction process.

Case II: Similar to the developments in case I, the time-reversed pressure field in (7d) can be written as a convolution of $o(x,y)\sigma_1(x,y,z_0,t)$ with the normal derivative of the free-space Green's function on II:

$$p_{\mathrm{tr}}^{(2)}(\mathbf{r},t) = -2[o(x,y)\sigma_1(x,y,z_0,t)] \overset{***}{\underset{xyt}{}} \frac{\partial}{\partial z_s} \times g_f(x,y,z-z_s,t)\big|_{z_s=z_0}. \tag{15a}$$

Taking the Fourier transform of (15a) over x, y, and t, it follows from (10) and (13c) that

$$\tilde{P}_{\mathrm{tr}}^{(2)}(f_x,f_y,z,f) = -\frac{j}{2}\exp(j2\pi fT)\tilde{\phi}(f)^* \exp(jvz_0)\exp(-jvz) \times \left(O(f_x,f_y) \overset{**}{\underset{f_x f_y}{}} \frac{1}{v^*} \exp(jvz_0)^* \right). \tag{15b}$$

Once again, the main difficulty is the computation of the convolution over f_x and f_y. If the size of the time-reversal mirror is large enough, such that $O(f_x,f_y)$ behaves like $\delta(f_x)\delta(f_y)$ compared to the variations of $\exp(jvz_0)^*/v^*$ with f_x and f_y, (15b) can be re-written as follows:

$$\tilde{P}_{\mathrm{tr}}^{(2)}(f_x,f_y,z,f) \simeq -(j/2v^*)\exp(j2\pi fT)\tilde{\phi}(f)^* \times |\exp(jvz_0)|^2 \exp(-jvz). \tag{15c}$$

Comparing (15c) with (14d), we note that the only difference is the substitution of v by its complex conjugate v^* in the amplitude coefficient $-j/2v$. Since v is either real or purely imaginary, the consequence is that the propagating components of the time-reversed pressure field are the same as in (14e), while the evanescent components are the opposite of those obtained in case I. Thus in case II we get:

$$\tilde{P}_{\mathrm{tr}}^{2}(f_x,f_y,z,f) \simeq -\frac{1}{4\pi}\exp(j2\pi fT)\tilde{\phi}(f)^* \begin{cases} \dfrac{j}{\sqrt{f^2/c^2-f_r^2}} \exp[-j2\pi z\sqrt{f^2/c^2-f_r^2}], & \text{if } f_r < f/c, \\ \dfrac{-1}{\sqrt{f_r^2-f^2/c^2}} \exp[2\pi(z-2z_0)\sqrt{f_r^2-f^2/c^2}], & \text{if } f_r > f/c. \end{cases} \tag{15d}$$

Case III: As found from the time analysis for case III, Eq. (8b) reveals that the pressure field is equal to half the sum of the pressure fields found for cases I and II, plus a correction term. Assuming that this correction term is negligible, $\tilde{P}_{\mathrm{tr}}^{(3)}(f_x,f_y,z,f)$ can be written as

$$\tilde{P}_{\mathrm{tr}}^{(3)}(f_x,f_y,z,f) = \tfrac{1}{2}\tilde{P}_{\mathrm{tr}}^{(1)}(f_x,f_y,z,f) + \tfrac{1}{2}\tilde{P}_{\mathrm{tr}}^{(2)}(f_x,f_y,z,f). \tag{16a}$$

Further assuming that the convolution terms in (14c) and (15b) containing $O(f_x,f_y)$ can be ignored (same as done in cases I and II), we obtain

$$\tilde{P}_{\mathrm{tr}}^{(3)}(f_x,f_y,z,f) \simeq -\frac{j}{4}\left(\frac{1}{v}+\frac{1}{v^*}\right)\exp(j2\pi fT)\tilde{\phi}(f)^* \times |\exp(jvz_0)|^2 \exp(-jvz). \tag{16b}$$

Once again, this expression is very similar in form to (14d) and (15c). It also follows from (16b) that the propagating components of the time-reversed pressure field are the same as in (14e) and (15d), while the sum of the evanescent components is zero. This result has been observed in holographic techniques and is in complete agreement with previous works.[18–22]

Case IV: As mentioned in the previous section, this case is similar to case I. Replacing the secondary source term σ_0 by σ_1, we obtain

$$p_{\mathrm{tr}}^{(4)}(\mathbf{r},t) = 2[o(x,y)\sigma_1(x,y,z_0,t)] \overset{***}{\underset{xyt}{}} g_f(x,y,z-z_0,t). \tag{17a}$$

Taking the Fourier transform of (17a) over x, y, and t, we immediately obtain[13]

$$\tilde{P}_{\mathrm{tr}}^{(4)}(f_x,f_y,z,f) = (1/2v)\exp(j2\pi fT)\tilde{\phi}(f)^* \exp(jvz_0)\exp(-jvz) \times \left(O(f_x,f_y) \overset{**}{\underset{f_x f_y}{}} \frac{1}{v^*} \exp(jvz_0)^* \right). \tag{17b}$$

As done in cases I and II, if the convolution term in (17b) containing $O(f_x,f_y)$ can be ignored, the simplification yields

$$\tilde{P}_{\mathrm{tr}}^{(4)}(f_x,f_y,z,f)$$
$$\simeq(1/2|v|^2)\exp(j2\pi fT)\tilde{\phi}(f)^*|\exp(jvz_0)|^2$$
$$\times\exp(-jvz). \tag{17c}$$

In conclusion, when considering the different expressions for the Fourier transforms of the time-reversed pressure fields in (14d), (15c), (16b) and (17c) corresponding to the four cases above, we can make the following conclusions.

(1) In the frequency domain, all the expressions contain the same term $\exp(j2\pi fT)\tilde{\phi}(f)^*$, thus in the time domain, the time-reversed pressure field varies linearly (in the frame of the linear system theory) with respect to $\phi(T-t)$, and not with respect to $\phi(t)$.[2,5]

(2) Except for case IV, the reconstruction of the propagating components of the time-reversed pressure field depends neither on the baffle conditions (rigid, soft or free-space), nor on the position z_0 of the time-reversal mirror.

(3) The only observable difference between the three baffle conditions (cases I, II, and III) is the evanescent components of the time-reversed field; since these components decrease exponentially with z, it is foreseeable that this difference tends to be insignificant when z_0 is great enough compared to the wavelength $\lambda=c/f$.

III. PARTICULAR CASES

This section considers some particular cases for which closed form solutions are available for the time-reversed pressure field.

More specifically, we will consider case III introduced in the two previous sections, i.e., corresponding to the free-space Green's function. We assume that the mirror is large enough such that the correction term (integration over $\mathscr{P}$) in (8b) is negligible, and the convolution terms containing $O(f_x,f_y)$ in (14c) and (15b) can be ignored. These assumptions are supposed to be valid in the frequency range of the excitation function $\phi(t)$. Under such conditions, (16b) is valid and can be re-written, with v inserted, as follows:

$$\tilde{P}_{\mathrm{tr}}^{(3)}(f_x,f_y,z,f)=-\frac{j\exp(j2\pi fT)\tilde{\phi}(f)^*}{4\pi\sqrt{f^2/c^2-f_r^2}}$$
$$\times\exp(-j2\pi z\sqrt{f^2/c^2-f_r^2})$$
$$\times\Theta(f/c-f_r), \tag{18a}$$

where $\Theta(\cdots)$ is the Heaviside step function. In (18a), the time-reversed pressure field only depends on f_r and will subsequently be written as $\tilde{P}_{\mathrm{tr}}^{(3)}(f_r,\cdot,z,f)$. It follows from the radial symmetry that the time-reversed pressure field in the space and frequency domain, $\tilde{p}_{\mathrm{tr}}^{(3)}(x,y,z,f)$, also has radial symmetry[13] and only depends on $r=\sqrt{x^2+y^2}$: it will subsequently be written as $\tilde{p}_{\mathrm{tr}}^{(3)}(r,\cdot,z,f)$. In this case, the forward and inverse spatial two-dimensional Fourier transforms are identical and reduce to a Hankel transform using the Bessel function of zeroth order:[13,14]

$$\tilde{p}_{\mathrm{tr}}^{(3)}(r,\cdot,z,f)=2\pi\int_0^{+\infty}\tilde{P}_{\mathrm{tr}}^{(3)}(f_r,\cdot,z,f)$$
$$\times f_r J_0(2\pi rf_r)df_r. \tag{18b}$$

We will now show that we can obtain a closed form solution for the time-reversed pressure field $\tilde{p}_{\mathrm{tr}}^{(3)}(r,\cdot,z,f)$ in the two following cases: $z=0$ (the xy plane) and $r=0$ (the z axis). We first consider the case $z=0$; this corresponds to an observation point located in the xy plane, parallel to the mirror, that contains the source (see Fig. 1). Inserting (18a) into (18b) and setting $z=0$ yields

$$\tilde{p}_{\mathrm{tr}}^{(3)}(r,\cdot,z=0,f)=\frac{\exp(j2\pi fT)\tilde{\phi}(f)^*}{2j}$$
$$\times\int_0^{f/c}\frac{f_r}{\sqrt{f^2/c^2-f_r^2}}J_0(2\pi rf_r)df_r. \tag{19a}$$

The value of the integral over f_r can be found in tables of integral transforms;[15] it reduces to the spherical Bessel function[14] $\sin(2\pi rf/c)/2\pi r$. It follows therefore that the time-reversed pressure field $\tilde{p}_{\mathrm{tr}}^{(3)}(r,\cdot,z=0,f)$ is given by

$$\tilde{p}_{\mathrm{tr}}^{(3)}(r,\cdot,z=0,f)=\frac{1}{2j\lambda}\frac{\sin(kr)}{kr}\exp(j2\pi fT)\tilde{\phi}(f)^*, \tag{19b}$$

where k is the wave number defined by $k=2\pi/\lambda$. Taking the inverse Fourier transform of (19b) over the frequency variable f, we obtain[13]

$$p_{\mathrm{tr}}^{(3)}(r,\cdot,z=0,t)=\frac{1}{8\pi r}\phi\left(T-t-\frac{r}{c}\right)-\frac{1}{8\pi r}\phi\left(T-t+\frac{r}{c}\right). \tag{19c}$$

Comparing (19b) and (19c) to the two corresponding equations for the CTRC system in a homogeneous fluid,[2,5] we observe that they are pairwise identical, apart from an amplitude factor 1/2. The time-reversed pressure field behaves as the superposition of two spherical waves, one converging to and one diverging from the source. Observed over time, the time-reversed pressure field exhibits two different wave fronts, where the second is an exact replica of the first, except that it is time-shifted and multiplied by -1. As in the CTRC system, the two wave fronts can overlap near the origin ($x\simeq0$, $y\simeq0$, $z=0$), while they are completely separated in time far from the origin. At a given frequency, the maximum available resolution for the focusing process by time-reversal is $\lambda/2$.[2,5,18–22]

We next consider the case $r=0$; this corresponds to an observation point located on the z axis, perpendicular to the surface of the mirror, that contains the source (see Fig. 1). Inserting (18a) into (18b) and setting $r=0$ yields

$$\tilde{p}_{\mathrm{tr}}^{(3)}(r=0,\cdot,z,f)$$
$$=\frac{\exp(j2\pi fT)\tilde{\phi}(f)^*}{2j}\int_0^{f/c}\frac{f_r}{\sqrt{f^2/c^2-f_r^2}}$$
$$\times\exp(-j2\pi z\sqrt{f^2/c^2-f_r^2})df_r. \tag{20a}$$

Making the change of integration variable defined by $\xi^2=f^2/c^2-f_r^2$, we obtain, after some intermediate steps, the following expression:

$$\tilde{p}_{\mathrm{tr}}^{(3)}(r=0,\cdot,z,f)=\frac{1}{2j\lambda}\exp\left(-j\frac{\pi z}{\lambda}\right)\frac{\sin(kz/2)}{kz/2}\times\exp(j2\pi fT)\tilde{\phi}(f)^*. \tag{20b}$$

Taking the inverse Fourier transform of (20b) over the frequency variable f, we obtain[13]

$$p_{\mathrm{tr}}^{(3)}(r=0,\cdot,z,t)=\frac{1}{4\pi z}\phi\left(T-t-\frac{z}{c}\right)-\frac{1}{4\pi z}\phi(T-t). \tag{20c}$$

Finally, comparing (19b), (19c), (20b) and (20c), we find some important differences.

(1) Equation (20b) contains a phase term $\exp(-j\pi z/\lambda)$ varying with z; this term is due to the propagation of the pressure field along the z axis, which is perpendicular to the surface of the mirror.

(2) Equation (19b) shows an amplitude variation $\sin(kr)/kr$ while (20b) shows a similar variation $\sin(kz/2)/(kz/2)$; the minimum obtainable resolution size along the z axis is twice the size along the r-axis.

(3) Equation (19c) contains two symmetrical wave fronts described geometrically by equations of the form $t=C\mp r/c$, where C is a constant whose exact value is unimportant in this context.

(4) Similarly, (20c) shows two different wave fronts, but they are not symmetrical; they are described geometrically by equations of the form $t=C-z/c$ and $t=C$, respectively, and one of these two wave fronts has a geometrical shape that does not depend on z.

It is important to note that these results are valid theoretically only in the case of the free-space Green's function. But as mentioned above, the only difference between the three baffle conditions (cases I, II, and III) lies in the reconstruction of the evanescent components of the time-reversed field. As a consequence, these results can be extended to cases I and II introduced in the previous sections (i.e., for the hard and soft baffle conditions) if the evanescent components of the time-reversed pressure field are negligible. This condition is satisfied as long as the distance z_0 between the source and the time-reversal mirror is large compared to the greatest wavelength corresponding to the frequency range of the excitation function $\phi(t)$.

In order to increase the performance of the focusing process on the source by time-reversal, we introduce a second time-reversal mirror, identical to the first one, located in the plane $z=z_1$ where $z_1<0$, and synchronized in time with the first mirror. The parameter T, introduced in the first section, is identical for the two mirrors and corresponds to that mirror furtherst away from the source. Continuing with case III (the free-space Green's function), it must be noted that *the time-reversed pressure field does not depend on the position of the mirror.* It follows therefore, and from elementary symmetry properties of the second mirror with respect to the first one, that the contribution of the second mirror to the total time-reversed pressure field at z is identical to the contribution of the first mirror at $-z$ (symmetry around the source). Adding these two contributions, we immediately obtain from (16b) the following expression:

$$\tilde{P}_{\mathrm{tr}}^{(3)}(f_r,\cdot,z,f)=-\frac{j\exp(j2\pi fT)\tilde{\phi}(f)^*}{2\pi\sqrt{f^2/c^2-f_r^2}}\times\cos(2\pi z\sqrt{f^2/c^2-f_r^2})\Theta(f/c-f_r). \tag{21a}$$

The Hankel transform of this function with respect to f_r can be found in tables of integral transforms,[15] thus leading to

$$\tilde{p}_{\mathrm{tr}}^{(3)}(r,\cdot,z,f)=\frac{1}{j\lambda}\frac{\sin(k\sqrt{r^2+z^2})}{k\sqrt{r^2+z^2}}\exp(j2\pi fT)\tilde{\phi}(f)^*. \tag{21b}$$

Finally taking the inverse Fourier transform of (21b) over the frequency variable f, we return to the space and time domain and obtain[13]

$$p_{\mathrm{tr}}^{(3)}(r,\cdot,z,t)=\frac{1}{4\pi R}\phi\left(T-t-\frac{R}{c}\right)-\frac{1}{4\pi R}\phi\left(T-t+\frac{R}{c}\right), \tag{21c}$$

with $R=\sqrt{r^2+z^2}$. In this case, the total time-reversed pressure field resulting from two mirrors located around the source is spherically symmetric and corresponds exactly to the result obtained with the CTRC system.[2,5] These different results can be interpreted as follows.

(1) Using one or two mirrors, the radial dimension of the focal pattern is unchanged and identical to the result obtained with the CTRC system: since the mirror(s) is (are) assumed to be infinite (or very large), all the radial components of the initial pressure field are measured and effectively time-reversed.

(2) Using only one mirror, the axial extent (z axis) of the focal pattern is twice that of the radial extent (r axis): this is due to the fact that the z direction is preferred by a single mirror configuration and the only components of the initial pressure field that propagate in direction of increasing values of z are measured and time-reversed.

(3) In the two-mirror configuration, all the components of the initial pressure field are effectively measured and time-reversed, thus leading to results which are equivalent to those obtained with the CTRC system working in a homogeneous fluid.

It follows, therefore, that the use of two time-reversal mirrors, located on each side of the source, increases the performance of the focusing process in comparison with a single mirror configuration. Such a setup behaves exactly like a closed surface mirror, and this conclusion is coherent with previous works, which have found that the reconstructed field does not depend on the geometrical shape of the cavity.[2,5,18–22]

IV. NUMERICAL RESULTS

In order to illustrate the effects of the different parameters (radiation conditions on the surface of the mirror,

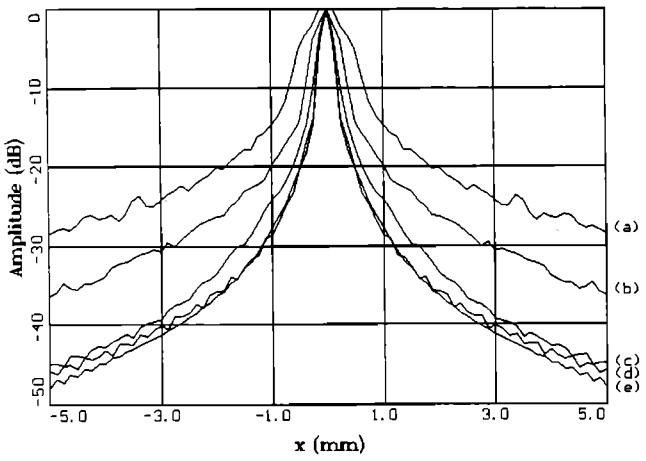

FIG. 2. Maximum temporal amplitude of the time-reversed pressure field as a function of x, $y=z=0$ mm, using a plane square mirror located at $z_0=20$ mm. Curves (a), (b), (c), (d), and (e) correspond to a mirror of dimension $a=10$ mm, $a=20$ mm, $a=40$ mm, $a=80$ mm, and $a=160$ mm, respectively.

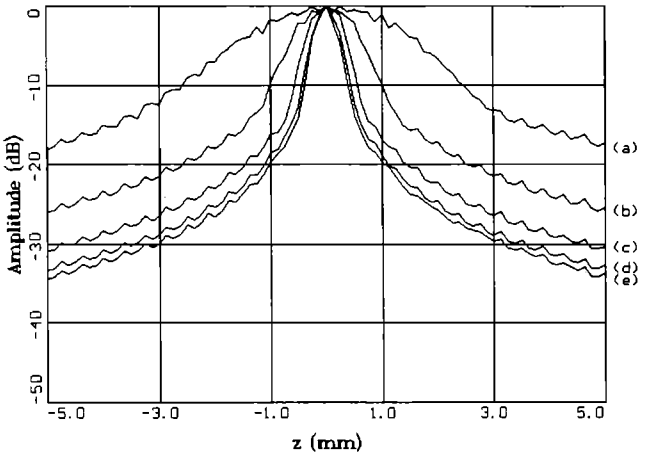

FIG. 3. Maximum temporal amplitude of the time-reversed pressure field as a function of z, $x=y=0$ mm, using a plane square mirror located at $z_0=20$ mm. Curves (a), (b), (c), (d), and (e) correspond to a mirror of dimension $a=20$ mm, $a=40$ mm, $a=80$ mm, $a=160$ mm, and $a=320$ mm, respectively.

size of the mirror) on the time-reversed pressure field, equations (6e), (7f) and (9) have been evaluated numerically. The integrals are computed by use of classical *Simpson's integration rule* with a spatial sampling of the function to integrate.[23,24] The computations are performed in the time domain, using 256 temporal points with a sampling frequency of 20 MHz. The sound speed c is 1500 m/s. The excitation function $\phi(t)$ is a sinusoidal burst with a Gaussian envelope function, explained in detail in the Appendix. The center frequency of $\phi(t)$ is 3 MHz and its relative -6-dB bandwidth is 100%. The spatial sampling on the surface of the time-reversal mirror is defined by steps $\Delta x=\Delta y=0{,}1$ mm, corresponding to fifth the center wavelength in the frequency range of the excitation function (in a first step, we have checked the validity of these values, taking into account the other parameters of the problem). In the following, we consider square time-reversal mirrors, with side length a, that are located such that the z axis intersects the center of the mirror.

We first consider a square time-reversal mirror located at $z_0=20$ mm. The time-reversed pressure field is computed between $x=-5$ mm and $x=+5$ mm, $y=z=0$ mm. The boundary conditions on the surface of the mirror are those corresponding to case I introduced in the first and second sections of this paper. At each observation point, the maximum temporal amplitude is evaluated and represented as a function of x. The results are shown in Fig. 2. Curves (a), (b), (c), (d), and (e) correspond to a mirror of dimension $a=10$ mm, $a=20$ mm, $a=40$ mm, $a=80$ mm, and $a=160$ mm, respectively. We observe a significant difference between curves (a) and (e), and how the focal pattern narrows as the size of the time-reversal mirror increases. Curves (d) and (e) are completely identical between -35 and 0 dB, while they exhibit insignificant difference in the range [-50 dB, -35 dB]. The *plots* also show how the focal pattern converges to the ideal focal pattern of an infinite time-reversal mirror. From Fig. 2, the width of the ideal focal pattern, measured at -10 dB, is about 0,38 mm.

Similar to Fig. 2, the time-reversed pressure field is computed between $z=-5$ mm and $z=+5$ mm, $x=y=0$ mm, and the maximum temporal amplitude is represented as a function of z in Fig. 3. The boundary conditions on the surface of the mirror are the same as above. Curves (a), (b), (c), (d), and (e) correspond to a mirror of dimension $a=20$ mm, $a=40$ mm, $a=80$ mm, $a=160$ mm, and $a=320$ mm, respectively. The effect of the size of the mirror appears clearly, as the focal pattern narrows as the size of the mirror increases. As in Fig. 2, we see that the focal pattern converges to the ideal focal pattern of an infinite time-reversal mirror, but the convergence is not as rapid as in the previous case. From Fig. 3, the width of the ideal focal pattern, measured at -10 dB, is about 0,75 mm, which is twice the width obtained from Fig. 2. This is

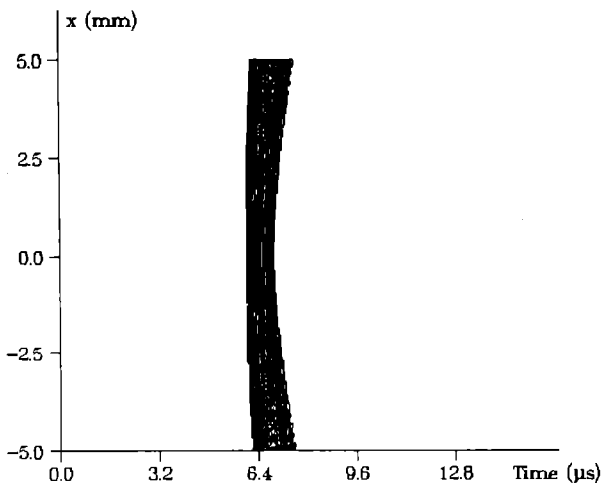

FIG. 4. Time-reversed pressure field using a mirror of dimension $a=5$ mm located at $z_0=20$ mm. The observation point varies from $x=-5$ mm to $x=+5$ mm, $y=z=0$ mm, and the amplitude of the field is converted to dB units in the range [-50 dB, 0 dB].

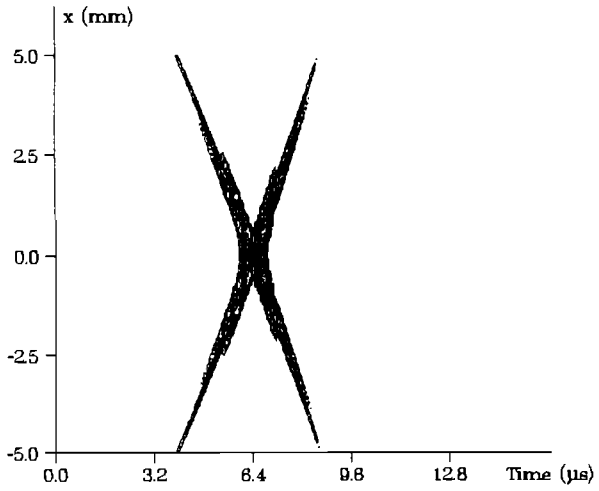

FIG. 5. Time-reversed pressure field, same as Fig. 3, but using a mirror of dimension $a=40$ mm.

consistent with the theoretical results obtained in the third section of this paper.

A computation similar to the one above has been performed with a time-reversal mirror of smaller dimension, where $a=5$ mm. The pressure field is now observed as a function of time and space, where the spatial observation point varies from $x=-5$ mm to $x=+5$ mm, $y=z=0$ mm. The amplitude of the time-reversed pressure field is converted to dB units in the range [−50 dB, 0 dB] and the result obtained is represented in Fig. 4 as a contour plot. The pressure field shows a single wave front whose geometrical shape appears quadratic. This observation can be verified by consulting, for example, (6e) and considering the time-reversal mirror to be point-like. In (6e), the two vectors $\mathbf{r}$ and $\mathbf{r}_s$ are given by their coordinates $\mathbf{r}(x,0,0)$ and $\mathbf{r}_s(0,0,z_0)$, so the geometry of the resulting wave front is described by an equation of the form $ct = C + \sqrt{x^2+z_0^2} - z_0$. This equation corresponds to the spherical wave front generated by a point-like time-reversal mirror and we note here the quadratic shape visible in Fig. 4.

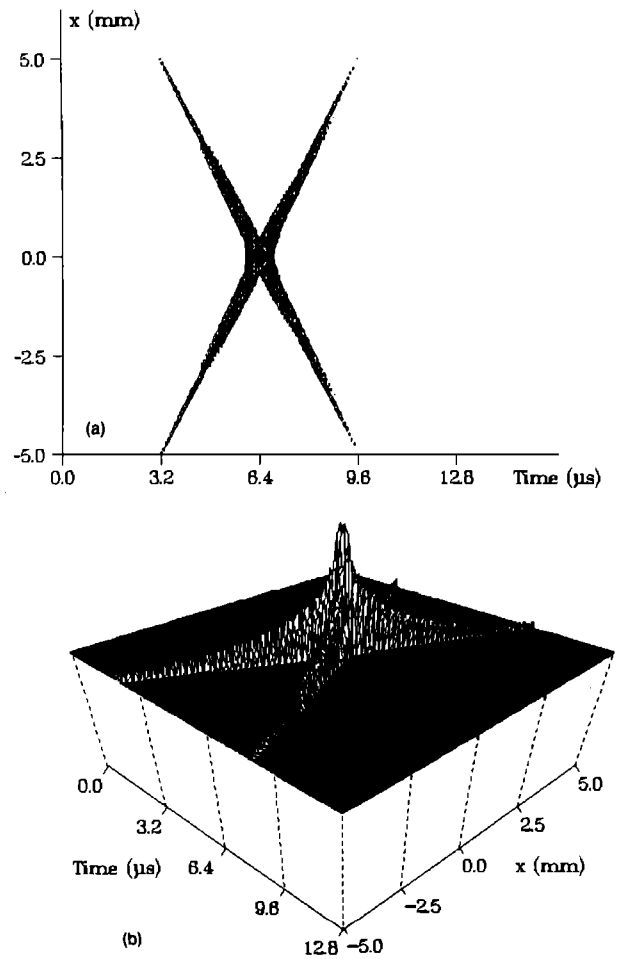

FIG. 6. Time-reversed pressure field using a mirror of dimension $a=160$ mm: (a) contour plot, (b) 3-D representation.

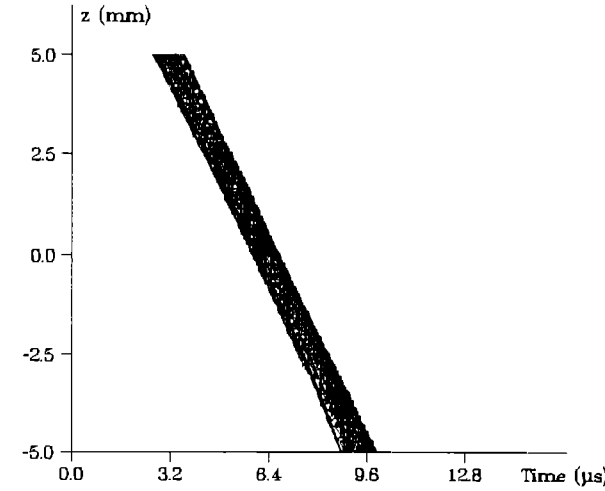

FIG. 7. Time-reversed pressure field using a mirror of dimension $a=20$ mm. The observation point varies from $z=-5$ mm to $z=+5$ mm, $x=y=0$ mm and the amplitude of the field is converted to dB units in the range [−50 dB, 0 dB].

In Fig. 5, the time-reversed pressure field is computed and represented in the same way as above, but the size of the mirror is now $a=40$ mm. This plot shows two different wave fronts; geometrically, they can almost be represented by symmetrically straight lines. The slopes of these straight lines are about ± 2.13 mm/μs.

Finally, the time-reversed pressure field obtained with a mirror of dimension $a=160$ mm is shown in Fig. 6(a). The two wave fronts observed in Fig. 5 are still present, but they are now, geometrically, completely linear and symmetric with slopes of about ± 1.56 mm/μs. This value is very close to the theoretical slope that can be predicted according to the third part of this paper with an infinite time-reversal mirror: $c=1.5$ mm/μs. In Fig. 6(b), the pressure field is represented in 3-D; in this figure, we clearly see how the time-reversed pressure field is focused on the source; the two wave fronts and the overlap effect near the origin are also visible.

Figures 7, 8, and 9 are equivalent to Figs. 4, 5, and 6, but they apply time-reversal mirrors of dimension $a=20$ mm, $a=80$ mm, and $a=320$ mm, respectively. The observation point varies from $z=-5$ mm to $z=+5$ mm, $x=y=0$ mm. In Fig. 7, we note that the pressure field

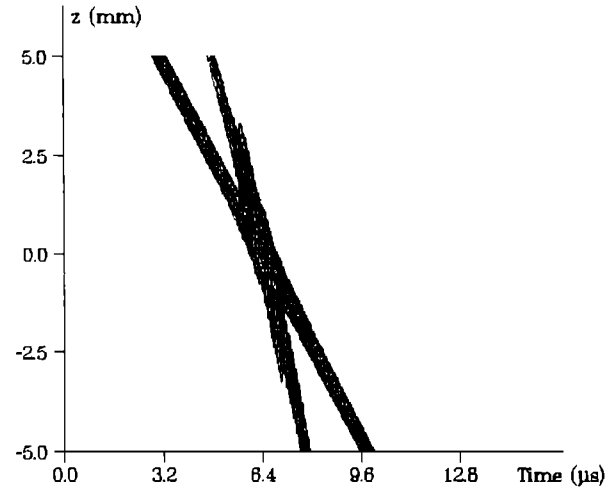

FIG. 8. Time-reversed pressure field using a mirror of dimension $a=80$ mm. Otherwise, same conditions as Fig. 7.

shows a single straight wave front with a slope of about -1.56 mm/μs. As above, we can consider (6e), for example, and assume that the time-reversal mirror is point-like. In this case, the two vectors $\mathbf{r}$ and $\mathbf{r}_s$ are given by their coordinates $\mathbf{r}(0,0,z)$ and $\mathbf{r}_s(0,0,z_0)$, such that the resulting

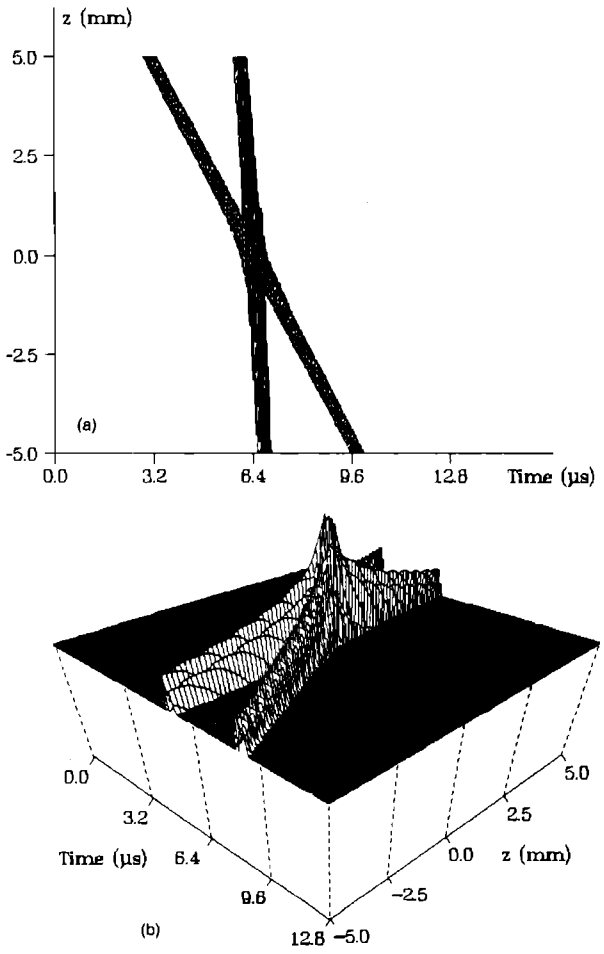

FIG. 9. Time-reversed pressure field using a mirror of dimension $a=320$ mm: (a) contour plot, (b) 3-D representation.

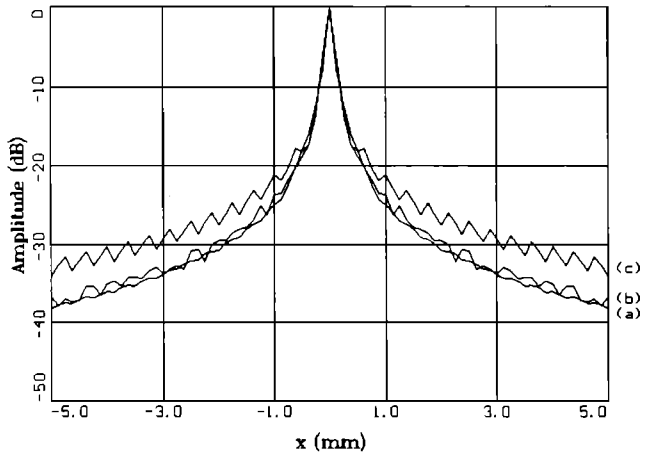

FIG. 10. Maximum amplitude of the time-reversed pressure field as a function of x, $y=z=0$ mm, using a plane square mirror of dimension $a=20$ mm located at $z_0=0.1$ mm. Curves (a), (b), and (c) correspond to cases I, II, and IV (radiation conditions) introduced in the first section, respectively.

wave front is described by an equation of the form $ct=C-z$. This result is consistent with the approximate value of the slope of the straight wave front. As in Fig. 5, the time-reversed pressure field represented in Fig. 8 shows two straight wave fronts; their slopes are about -1.56 mm/μs and -7.14 mm/μs, respectively. Also in Fig. 9, two wave fronts are present. One of them has a slope of about -1.56 mm/μs while the second is almost vertical, thus resulting in an infinite slope and a wave front whose geometrical shape does not depend on z. Once again, these results are in perfect agreement with the theoretical predictions in the third part of this paper in the case of an infinite time-reversal mirror.

Finally, we consider the influence of the radiation conditions on the surface of the mirror. If we compare the different expressions for the time-reversed pressure field given by (6e), (7f) and (9), we see that the temporal variation and the decrease of the amplitude of the time-reversed pressure field vary from one radiation condition to another, but the geometrical shapes of the wave fronts are unchanged. It is also foreseeable from these equations that the relative influence on the amplitude of the field decreases as the distance z_0 between the source and the mirror increases. This observation is consistent with the remarks made in the second section and with other numerical results not presented in this paper. Similar to the previous computations, we consider a time-reversal mirror of dimension $a=20$ mm located very near the source: $z_0=0.1$ mm. The maximum temporal amplitude of the field is converted to dB units in the range [-50 dB, 0 dB] and the observation point varies from $x=-5$ mm to $x=+5$ mm, $y=z=0$ mm. Figure 10 reveals the results with radiation conditions corresponding to cases I [curve (a)], II [curve (b)] and IV [curve (c)] introduced in the first section, respectively. From this figure, we make the following observations.

(1) The three focal patterns are identical in the range [-15 dB, 0 dB]: the time-reversed pressure field is focused

on the source and the size of the focal zone does not change.

(2) Except for some small oscillations, due to the finite spatial sampling frequency used to describe the surface of the mirror for the numerical computation of the field, we cannot observe any significant difference between curves (a) and (b): this is consistent with the theoretical predictions of the second section of this paper based on the frequency analysis of the time-reversed pressure field.

(3) Comparing curve (c) with (a) and (b), we clearly see that the maximum amplitude of the time-reversed pressure field decreases more rapidly with the distance between the source and the observation point in cases I and II than in case IV: considering (6e), (7f) and (9), such an effect was also foreseeable.

These results are very important since they prove that, except for the particular case of a time-reversal mirror located very near the source, there are no significant differences between the focal patterns obtained with the different radiation conditions analyzed here. This result is particularly interesting in case IV that corresponds to the most realistic configuration from an experimental point of view, and we can see that the focal pattern is not altered in a drastic way. All these results allow the consideration of the plane time-reversal mirrors as an efficient alternative to closed cavities.

V. CONCLUSION

In this paper, we have presented a theoretical and numerical model for focusing of ultrasonic fields by means of the time-reversal technique using plane mirrors of finite dimension in a homogeneous fluid. Specifically, we have shown that the use of a single mirror of finite size, *that does not surround* the focal spot, reduces the focusing efficiency when compared to that which can be obtained theoretically with the CTRC system. The focusing efficiency also decreases with the size of the time-reversal mirror as we measure and time-reverse more information coming from the source using a greater mirror. The differences between the radiation conditions on the surface of the mirror are completely negligible, except when the distance between the source and the mirror is small compared to the wavelength. In this case, the evanescent components of the pressure field are still present and observable, and have a significant contribution to the focal pattern generated by time-reversal. Although the time-reversal mirror, as presented in this paper, is not completely realizable experimentally, this work proves the efficiency of this kind of mirrors as an alternative to the CTRC system. In particular, the dimension of the mirror is an important parameter that can alter significantly the focusing efficiency if it is chosen too small. Based on the results presented in this paper, we are now working on experimental realizations of these kind of mirrors using 1-D and 2-D transducer arrays.

ACKNOWLEDGMENTS

The authors would like to thank Dr. Jens E. Wilhjelm, The Electronics Institute, Technical University of Denmark, for helpful discussions in preparation of this manuscript.

APPENDIX: MODEL FOR THE EXCITATION FUNCTION

The excitation function $\phi(t)$ is computed according to the following formula:

$$\phi(t)=\sin(2\pi f_0 t)\exp[-(t-T_\phi/2)^2/\sigma^2] \times \mathrm{rect}_{T_\phi}(t-T_\phi/2),$$

where

(i) f_0 is the central frequency of the signal: $f_0=3$ MHz;

(ii) the relative bandwidth at -6 dB is B, such that the significant frequency range (it is assumed to be symmetrical) is $[(1-B/2)f_0,(1+B/2)f_0]$; once this parameter is defined ($B=100\%$), it is easy to compute the parameter σ as

$$\sigma^2=4\ln 2/\pi^2 f_0^2 B^2 \simeq 3.12\times 10^{-2}\ \mu\mathrm{s}^2;$$

(iii) the function $\mathrm{rect}_{T_\phi}(t)$ insures that the excitation function $\phi(t)$ is only defined on the finite time interval $[0,T_\phi]$; it is defined by

$$\mathrm{rect}_{T_\phi}(t)=\begin{cases}1, & \text{if } -T_\phi/2\leqslant t\leqslant +T_\phi/2,\\ 0, & \text{if } t<-T_\phi/2 \text{ or } t>+T_\phi/2;\end{cases}$$

(iv) the width T_ϕ of the finite time support of the excitation function is chosen such that the gaussian modulation of the amplitude is less than the maximum precision available with numerical floating point values (10^{-7}) outside this interval:

$$T_\phi=2\sigma\sqrt{7\ln 10}\simeq 1.42\ \mu\mathrm{s}.$$

This choice insures that the excitation function $\phi(t)$ computed numerically does not show any discontinuity.

[1] M. Fink, C. Prada, F. Wu, and D. Cassereau, "Self-focusing in inhomogeneous media with time-reversal acoustic mirrors," Proc. IEEE Ultrason. Symp., 681–686 (1989).

[2] D. Cassereau, F. Wu, and M. Fink, "Limits of self-focusing using closed time-reversal cavities and mirrors—Theory and experiment," Proc. IEEE Ultrason. Symp., 1613–1618 (1990).

[3] M. Fink, "Time-reversal of ultrasonic fields—Part I: Basic principles," IEEE Trans. Ultrason. Ferroelec. Freq. Control **39**, 555–566 (1992).

[4] F. Wu, J. L. Thomas, and M. Fink, "Time-reversal of ultrasonic fields—Part II: Experimental results," IEEE Trans. Ultrason. Ferroelec. Freq. Control **39**, 567–578 (1992).

[5] D. Cassereau and M. Fink, "Time-reversal of ultrasonic fields—Part III: Theory of the closed time-reversal cavity," IEEE Trans. Ultrason. Ferroelec. Freq. Control **39**, 579–592 (1992).

[6] P. M. Morse and K. U. Ingard, *Theoretical Acoustics* (McGraw Hill, New York, 1968).

[7] M. Born and E. Wolf, *Principles of Optics* (Pergamon, New York, 1975).

[8] B. B. Baker and E. T. Copson, *The Mathematical Theory of Huygen's Principle* (Clarendon, Oxford, 1949).

[9] P. R. Stepanishen, "Transient radiation from pistons in an infinite planar baffle," J. Acoust. Soc. Am. **49**, 1629–1638 (1971).

[10] G. R. Harris, "Review of transient field theory for a baffled planar piston," J. Acoust. Soc. Am. **70**, 10–20 (1981).
[11] G. R. Harris, "Transient field of a baffled planar piston having an arbitrary vibration amplitude distribution," J. Acoust. Soc. Am. **70**, 186–204 (1981).
[12] R. L. Pritchard, "Mutual acoustic impedance between radiators in an infinite rigid plane," J. Acoust. Soc. Am. **32**, 730–737 (1960).
[13] A. Papoulis, *Signal Analysis* (McGraw-Hill, New York, 1984).
[14] G. Petiau, *La théorie des fonctions de Bessel* (Centre National de la Recherche Scientifique, Paris, 1955).
[15] H. Bateman, *Table of Integral Transforms* (McGraw-Hill, New York, 1954).
[16] D. Cassereau and D. Guyomar, "Reflection of an impulse spherical wave at a plane interface separating two fluids," J. Acoust. Soc. Am. **92**, 1706–1720 (1992).
[17] G. S. Agarwal and E. Wolf, "Theory of phase conjugation with weak scatterers," J. Opt. Soc. Am. **72**, 321–326 (1982).
[18] R. P. Porter and A. J. Devaney, "Holography and the inverse source problem," J. Opt. Soc. Am. **72**, 327–330 (1982).
[19] R. P. Porter, "Image formation with arbitrary holographic type surfaces," Phys. Lett. **29A**, 193–194 (1969).
[20] R. P. Porter, "Diffracted-limited, scalar image formation with holograms of arbitrary shape," J. Opt. Soc. Am. **60**, 1051–1059 (1970).
[21] R. P. Porter and A. J. Devaney, "Generalized holography and computational solutions to inverse source problems," J. Opt. Soc. Am. **72**, 1707–1713 (1982).
[22] E. Wolf and R. P. Porter, "On the physical contents of some integral equations for inverse scattering from inhomogeneous objects," Radio Sci. **21**, 627–634 (1986).
[23] P. J. Davis and P. Rabinowitz, *Methods of Numerical Integration* (Academic, New York, 1975).
[24] W. H. Press, B. P. Flannery, S. A. Teukolsky, and W. T. Vetterling, *Numerical Recipes in C* (Cambridge U.P., Cambridge, 1988).